Combined Quantum Mechanical/Molecular Mechanical Study on the Pentacoordinated Ferric and Ferrous Cytochrome $P450_{cam}$ Complexes

Ahmet Altun and Walter Thiel*

Max-Planck-Institut für Kohlenforschung, Kaiser-Wilhelm-Platz 1, D-45470 Mülheim an der Ruhr, Germany

Received: September 10, 2004; In Final Form: November 4, 2004

The pentacoordinated ferric and ferrous cytochrome $P450_{cam}$ complexes have been investigated by combined quantum mechanical/molecular mechanical (QM/MM) calculations in the presence of a protein/solvent environment and by QM calculations on the isolated QM regions with use of density functional theory. The B3LYP functional has been found more reliable than the BLYP and BHLYP functionals for estimating the relative state energies. The B3LYP/CHARMM calculations with an all-electron basis set for iron give high-spin ground states for the title complexes, in agreement with experiment. The comparison of the B3LYP/CHARMM results of the entire protein system with the B3LYP calculations on the naked QM regions shows that the amount of stabilization by the protein environment is largest for the intermediate-spin states, followed by the high-spin states of the complexes. The calculation of Mössbauer parameters in the presence of the enzyme environment confirms the double occupation of the d_{xz} orbital in the quintet spin state of the ferrous complex, consistent with the computed QM/MM energies in the enzyme environment, while the $d_{x^2-y^2}$ orbital is doubly occupied in the gas-phase quintet state.

I. Introduction

The cytochrome P450 enzymes, which constitute a superfamily of monooxygenases, are distributed ubiquitously in bioorganisms and catalyze many diverse vital reactions (oxidation, reduction, isomerization, dehydration, etc.) for regulating drug metabolism, biodegradation of xenobiotics, and biosynthesis of metabolites (cholesterol, steroids, etc.).[1] $P450_{cam}$ (CYP101), which catalyzes the regio- and stereospecific hydroxylation of camphor leading to 5-*exo*-hydroxycamphor as the sole product in the bacterium *Pseudomonas putida*, is the first as well as the best crystallographically characterized member of the P450 enzyme family due to its ready availability, aqueous solubility, and comparative ease of isolation and purification.[2] Thus, common knowledge regarding the various catalytic reactions of P450 proteins rests to a large extent on studies of $P450_{cam}$.

The P450 enzymes contain in their reactive site an iron−protoporphyrin IX complex (heme) bound to the protein via the thiolate sulfur of cysteinate (see Scheme 1). Their resting state (**1** in Scheme 1) is a water-bound[3,4] hexacoordinated low-spin[4−6] (LS) ferric complex. When a substrate enters the protein pocket, the water molecules, including the axially coordinated one, are displaced from the reactive center resulting in a high-spin[2,7,8] (HS) ferric pentacoordinated complex (**2** in Scheme 1). This process tunes the redox potential from −340 mV in **1** to −170 mV (−173 mV) in free (putidaredoxin-bound) **2** so that an electron from the reductase putidaredoxin, whose redox potential is −239 mV (−196 mV) in free (bound) form, can be accepted and, thus, the pentacoordinated HS ferrous complex (**3** in Scheme 1) is formed.[2,7,9] Hence, in the case of **2**, putidaredoxin binding modulates the difference in the redox potentials of reductase and **2** by only 1 kcal/mol (−69 mV vs −23 mV).[9] By contrast, putidaredoxin exhibits significant effector activity for a CO-bound $P450_{cam}$ complex.[10]

SCHEME 1

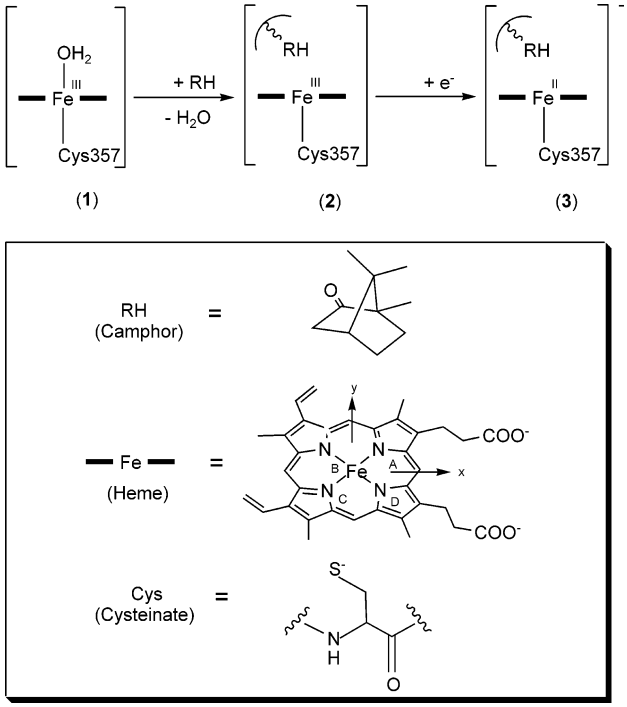

It is known experimentally[7,8,11,12] that the ground-state HS configuration mixes with the LS configuration in the pentacoordinated ferric $P450_{cam}$ complexes. The d-orbital occupations of the HS (sextet for the ferric and quintet for the ferrous) and LS (doublet for the ferric and singlet for the ferrous) states are shown in Scheme 2 together with the intermediate-spin (IS) configuration (quartet for the ferric and triplet for the ferrous complexes).

* To whom correspondence should be addressed. Phone: +49-208-306-2150. Fax: +49-208-306-2996. E-mail: thiel@mpi-muelheim.mpg.de.

10.1021/jp0459108 CCC: $30.25
Published on Web 12/30/2004

SCHEME 2

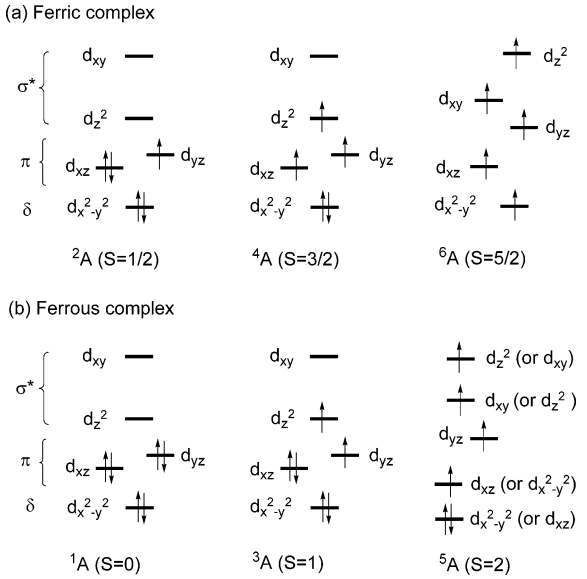

The computed relative energies of different spin states depend strongly on the choice of QM method. The quartet−sextet and doublet−sextet gaps of the ferric heme−SCH_3 complex (without heme substituents) in the gas phase have been calculated at the Hartree−Fock (HF) level of theory as 58 and 123 kcal/mol, respectively.[13] INDO/S semiempirical calculations in the gas phase yield quartet−sextet and doublet−sextet gaps of 3.18 and 18.12 kcal/mol for the ferric heme−SCH_3 complex (including substituents), respectively.[14] When the protein atoms are represented in the INDO/S calculations as AMBER point charges modifying the one-electron potential in the INDO Hamiltonian, the quartet−sextet and doublet−sextet gaps become 1.60 and 20.40 kcal/mol, respectively.[14] Thus, HF and INDO/S (with and without protein environment) calculations predict a sextet ground state for the ferric complex in agreement with experiment. Both methods give doublet−sextet gaps that are too high for spin equilibrium. Density functional theory (DFT) in the Kohn−Sham (KS) framework is known to provide realistic descriptions of the molecular structures and relative energies of both free-base and metal-containing porphyrin derivatives when using appropriate functionals and basis sets.[15,16] However, open-shell B3LYP/OPLS hybrid calculations on the pentacoordinated ferric complex with the basis sets LACVP** for iron and 6-31G* for the remaining atoms of the QM region (full heme, Cys357, and camphor) give the quartet state 2.0 and 5.6 kcal/mol lower in energy than the sextet and doublet states, respectively.[17] In the gas phase, the same energy ordering is found[17] by using unrestricted (restricted) open-shell B3LYP calculations on the isolated QM regions at the protein geometry, the quartet state being lower in energy than the sextet and doublet states by 0.3 and 4.3 kcal/mol (0.2 and 2.9 kcal/mol), respectively. In contrast, other DFT calculations on gas-phase model systems yield a HS ground state for the pentacoordinated complexes. Unrestricted B3LYP calculations on the ferric and ferrous heme−SH complex (without side chains) in the gas phase with the LACV3P+*(6-311+G*)//LACVP(6-31G) basis set (i.e., LACVP and LACV3P+* for iron, and 6-31G and 6-311+G* for the remaining atoms) give the quartet−sextet, doublet−sextet, triplet−quintet, and singlet−quintet gaps as 4.21, 4.23, 9.39, and 14.08 kcal/mol, respectively.[18] In another gas-phase B3LYP study,[19] these gaps were estimated to be 12.03, 2.34, 7.56, and 11.29 kcal/mol on the heme−SCH_3 (without side chains) model by using an all-electron basis set for iron, and 6-31G* elsewhere. This latter DFT study differs from the others mainly in predicting a high-lying quartet state of the ferric complex. Although all of these B3LYP calculations estimate the doublet−sextet gap to be rather small, one may expect it to be even smaller to account for the observed spin equilibrium.

The present study reports combined quantum mechanical/molecular mechanical (QM/MM) calculations on the pentacoordinated ferric and ferrous P450$_{cam}$ complexes as well as pure DFT calculations on the isolated QM subsystems to probe the effect of the protein environment on relative energies, electronic structures, geometries, and Mössbauer parameters of each spin state. The treatment of exchange interactions in hybrid density functionals is known to affect the relative stability of different spin states.[20−23] Therefore, we have also examined the effect of exact exchange on the relative energies of each spin state of the ferric and ferrous complexes. The paper is organized as follows. The details of the computational protocol employed are described in section II. Section III presents the results of the computations. Section IV is devoted to the discussion of the results and concluding remarks.

II. Computational Methodology

A. Setup of the System. The monoclinic X-ray structures[11] of the ferric (resolution, 1.6 Å; PDB code, 1DZ4) and ferrous (resolution, 1.9 Å; PDB code, 1DZ6) pentacoordinated complexes of P450$_{cam}$ have very similar protein conformations around the reactive center compared with each other and with the orthorhombic X-ray structure[24] (resolution, 1.62 Å; PDB code, 2CPP) of the ferric complex. We chose the 1DZ4 structure as the starting point of our simulations. The missing hydrogen atoms and water molecules were added to the system. A series of molecular mechanics (MM) and molecular dynamics (MD) runs with the CHARMM force field[25] implemented in the CHARMM[26] program were carried out to relax the resulting ferric structure, which consists of 24 679 atoms (17 286 solvent atoms). The details of these classical force field calculations performed only for the ferric complex, in which the coordinates of heme, the coordinating Cys357, and the outer 8 Å of the solvent layer were kept fixed, are given in the Supporting Information.

B. Protonation State. The assignment of protons to titratable groups of the protein is done according to a previously defined standard protocol,[20] using the hbuild procedure of the CHARMM, published protonation states of P450$_{cam}$ based on Poisson−Boltzmann calculations,[27] and visual inspection of the environment of charged amino acids and histidine residues. The nonstandard assignments are as follows: (i) Glu366 was protonated at the carboxylate side chain.[27] (ii) The short distances between the two carboxylate functions of Asp297 and the A-propionate side chain in the X-ray structure suggest that these groups are linked by a H-bond. Asp297 was protonated at its OD2 atom since this atom has the shorter distance to the O2A atom of the propionate side chain of heme. The resting state study[20] shows that the relative spin state energies are not affected much by the protonation state of Asp297. (iii) The His80, His270, His308, His352, and His355 residues were protonated at both nitrogens. These five doubly protonated histidines form salt-links to Asp77, Glu269, Glu73, Glu76, and one of the propionate side chains of the heme. The remaining histidines are protonated at either the δ (residues 21, 62, 337, and 361) or ϵ (residues 17, 176, 347, and 391) nitrogens upon visual inspection of their environment. The resulting total charge of the ferric system is −9e. Thus, the ferrous system has −10e.

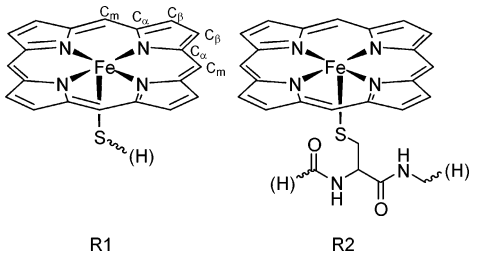

Figure 1. QM regions R1 and R2

This protonation pattern was also used for the resting state of $P450_{cam}$ [20] and is called Prot1. We neutralized the MM environment of one of the selected snapshots from the MD trajectory to probe the effect of the net charge in the MM region. There are many ways of neutralizing the MM environment. We selected the residues to be protonated among those that do not have artificial close contacts with the environment and do not change the MM environment significantly when a hydrogen atom is added. All the singly protonated histidines (see above) seem appropriate for this purpose. We chose these eight residues for protonation and also protonated Asp125. The resulting system (Prot2) has zero net charge. After adjusting the protonation state on a given snapshot to Prot2, an initial CHARMM minimization was performed keeping the coordinates of heme, the Cys357 residue, and the outer 8 Å of the solvent layer fixed, followed by full QM/MM optimization. The results presented in this study refer to Prot1 unless stated otherwise.

C. QM/MM and QM Calculations. We have investigated two randomly selected snapshots (after 31 and 93 ps of equilibration) of the MD trajectory with combined QM/MM calculations (full system) and pure QM calculations (reactive center only). The H-bond network around the reactive center is similar in these snapshots and in the X-ray structures (see section III.C). The following specifications apply to all calculations except those for the Mössbauer parameters which are described later (see section II.D).

1. QM Methods. Multireference ab initio approaches with sophisticated treatments of electron correlation are too expensive for the current system. Thus, we employed unrestricted KS (UKS) DFT calculations for the open-shell systems. Identical results were obtained from unrestricted and restricted KS calculations of the singlet ferrous complex, which thus represents a closed-shell system.

The BLYP, B3LYP, and BHLYP exchange-correlation functionals were applied, which combine Becke's 1988 (B88, no HF exchange),[28] Becke's three-parameter (B3, 20% HF exchange),[29] and Becke's half-and-half (BH, 50% HF exchange)[30] exchange functionals with the Lee−Yang−Parr (LYP)[31] correlation functional. All three exchange-correlation functionals were used in single-point calculations to assess the influence of the amount of HF exchange on the relative energies of the spin states. All QM geometry optimizations were done with the B3LYP functional.

2. QM Regions and Basis Sets. The QM/MM calculations were performed on two different QM regions (R1 and R2), which differ in the size of the chosen thiolate ligand (see Figure 1). The R1 model extends only to the sulfur atom of coordinating cysteinate, whereas the R2 model includes the full Cys357 residue, the CO group of Leu356, and the NH-C_αH unit of Leu358. Hydrogen link atoms[32] have been used to saturate the covalent bonds at the QM/MM border. Thus, the QM subsystems R1 and R2 consist of 39 and 56 atoms, respectively. Single-point calculations performed on larger QM regions including camphor, propionate side chains, and the residues with H-bonds to the propionates validate the appropriateness of the R1 and R2 regions in the enzyme and gas phase (see Section C6 of the Supporting Information).

The basis sets used are abbreviated as B1L, B2L, and B2W. L and W refer to the basis set at the iron atom, which is described either by a small-core effective core potential (ECP) together with the associated double-ζ quality LACVP basis[33] (L) or by Wachters all-electron basis set with an additional diffuse d function and a set of f polarization functions in the contraction [8s7p4d1f][34] (W). B1 employs the 6-31G basis on all atoms apart from iron whereas B2 includes also a set of diffuse and polarization functions (6-31+G*)[35] on the atoms coordinated to iron (four pyrrole nitrogens and the sulfur atom of cysteinate). Throughout this study, the QM level employed in a particular QM/MM calculation is denoted in the form QM region/basis set, e.g. R1/B1L, R2/B2W, etc. The consistency of the basis sets used was examined with single-point calculations which also used triple-ζ quality valence polarization (TZVP) basis sets.[36]

3. QM/MM Methods. An electronic embedding scheme[37] was applied, in which the fixed MM point charges are included in the one-electron Hamiltonian of the QM calculation and the QM/MM electrostatic interactions are evaluated from the QM electrostatic potential and the MM atomic charges. The electrostatic interactions between the QM region and the MM point charges were included in the QM energy whereas the van der Waals interaction between QM and MM atoms was calculated at the force field level and, thus, included in the MM energy. The QM/MM energy is the sum of QM and MM energies. No cutoffs were introduced for the nonbonding MM and QM/MM interactions. Hydrogen link atoms[32] were used to saturate covalent bonds cut at the QM/MM border and the charge shift model[38] was applied.

4. QM/MM Geometry Optimization. The QM/MM optimizations included all residues (including crystallographic and solvent waters) that have atoms within a distance of 4 Å around any atom of the heme−Cys357 complex and the substrate camphor. This region of 734 atoms comprised Phe87, Tyr96, Phe98, Pro100, Thr101, Gln108, Arg112, Ala115, Val119, Phe163, Leu244, Leu245, Val247, Gly248, Gly249, Thr252, Val253, Phe256, Leu289, Leu294, Val295, Asp297, Arg299, Gln322, Thr349, Phe350, Gly351, His355, Leu356, Leu358, Gly359, Gln360, Leu362, Ala363, Ile367, Ile395, Val396, the heme−Cys357 complex, substrate camphor, and crystallographic waters 63, 97, 252, 260, and 566, as well as one solvent water inside the protein.

Independent geometry optimizations of individual spin states for such large systems with high conformational complexity often result in conformations that have different protein/solvent environments. To exclude those artifacts, which are not related to the characteristics of the reactive center, we first performed QM/MM geometry optimizations for the sextet state of the ferric complex, and then the quintet state of the ferrous complex by adding one electron to the QM/MM optimized ferric complex. These geometries served as the starting point for geometry optimizations of the other spin states of the corresponding complex.

5. Gas-Phase Calculations. The QM regions of the QM/MM optimized structures were isolated and subjected first to single-point calculations, and then to full geometry optimizations to appreciate the influence of the protein environment on the QM subsystem. The former will be labeled as $S_{p,g}$ (the naked system at the protein geometry in the gas phase) and the latter as $S_{g,g}$

(the naked system optimized in the gas phase). The system with protein environment in the protein geometry will be denoted as $S_{p,p}$.

6. Codes. The ChemShell package[39,40] was utilized for the QM and QM/MM calculations. Both the pure QM and the QM part of the combined QM/MM calculations were performed by using the TURBOMOLE program.[41] The CHARMM22 force field[25] run through the DL-POLY program[42] was used for the treatment of the MM part of the system. The geometry minimizations were performed with the HDLC optimizer[43] in ChemShell.

D. Calculation of Mössbauer Parameters. The Mössbauer parameters of the pentacoordinated ferric and ferrous complexes were calculated by using the ORCA 2.2 program package.[44] For transition metal complexes, B3LYP is known to give more accurate Mössbauer parameters than GGA functionals such as BP86 mainly due to the larger spin polarization of the core induced by the HF exchange as well as a more realistic description of the metal−ligand covalency in the valence region.[45,46] Thus, B3LYP was used in the present study. The single-point calculations were performed on snapshot 93, which was optimized at the R2/B2L level for each spin state, and on the corresponding isolated QM region (R2) optimized at the same level in the gas phase. In the QM/MM single-point calculations, the electrostatic embedding scheme[37] was applied by using the MM point charges and their coordinates obtained previously from B3LYP/CHARMM optimizations at the R2/B2L level.

The calculation of the Mössbauer properties requires basis functions with high flexibility in the core region to account for spin polarization effects. In this study, the triply polarized (17s11p5d1f) → [17s7p3d1f] core properties basis set CP(PPP) was used for iron.[47] The SV(P) basis set was assigned to the remaining atoms leaving the inner s functions completely uncontracted.[36] An enhanced integration grid was used for iron and the overall integration accuracy was increased by using the "SpecialGridIntAcc=7" keyword in ORCA. The asymmetry parameter η and the Mössbauer quadrupole splitting ΔE_Q were calculated from the electric field gradient components (see ref 47 and references therein). The nuclear quadrupole moment Q of ^{57}Fe was taken as 0.15 barn. The Mössbauer isomer shift δ was evaluated from the electron density at the iron nucleus by using the correlation equation derived for the B3LYP functional.[47]

III. Results

A. Basis Set Dependence. B3LYP calculations with the B1L and B2L basis sets were successful in predicting the qualitative sequence of the relative state energies of the resting state and compound I of P450$_{cam}$.[20,48] For further basis set validation, we have performed B3LYP single-point calculations on the isolated R1 model system optimized at the B3LYP/B1L level by using the following basis sets: (i) B2L; (ii) B3T (all atoms described by TZVP); (iii) B2W; and (iv) B3W (Fe as in B2W, other atoms TZVP). The results are given in Table 1.

The energy order with the B1L basis (277 basis functions) is quartet < sextet < doublet for the neutral *ferric complex*. This changes to sextet < doublet < quartet with the addition of polarization and diffuse functions to the atoms coordinated to iron (B2L, 322 basis functions). When the flexibility of the core and valence regions is increased by using the TZVP basis set for all atoms (B3T, 589 basis functions), the energy order becomes sextet < quartet < doublet, and the relative energies change significantly compared with those for B1L and B2L.

TABLE 1: Basis Set Dependence of the Relative B3LYP State Energies (kcal/mol) of the Ferric and Ferrous Isolated R1 Model Complexes Computed on Geometries Optimized at the B3LYP/B1L Level

B1L	B2L	B3T	B3W	B2W
ferric complex: $[E(^4A) - E(^6A)]/[E(^2A) - E(^6A)]$				
−1.3/0.3	0.7/0.6	2.6/5.1	2.0/4.1	2.2/4.0
ferrous complex: $[E(^3A) - E(^5A)]/[E(^1A) - E(^5A)]$				
6.8/13.4	10.0/15.5	8.4/14.7	7.7/13.7	7.7/13.9

When the TZVP basis set at iron in B3T is replaced by a Wachters all-electron basis set with an additional set of diffuse d functions and f polarization functions (B3W, 612 basis functions), the relative energies of the higher spin states are lowered by 0.6−1.0 kcal/mol but the energy sequence is not altered. In an attempt to cut down the computational effort, we have also examined the B2W basis (356 basis functions), which combines the largest all-electron basis for iron (from B3W) and a smaller basis for the other atoms (from B2L). The results obtained with the B3W and B2W basis sets are practically the same, suggesting that B2 is adequate for the environment of the iron atom. Hence, B2W is our preferred basis for cost-effective and reliable calculations. It is used in the present study along with the smaller B1L and B2L basis sets. It should be noted in this context that previous B3LYP studies on the resting state[20,49] have also addressed basis set effects on relative spin state energies.

In the case of pentacoordinated *ferrous complex*, all five basis sets considered yield the same energy sequence (quintet < triplet < singlet) and similar gaps (see Table 1). B1L, B2L, and B2W reproduce the reference results from B3W with acceptable accuracy.

B. The Influence of HF Admixture. To assess the effect of exact exchange on the relative spin state energies in the absence and presence of protein environment (snapshot 93), we have utilized the B88 (no HF exchange), B3 (20% HF exchange), and BH (50% HF exchange) exchange functionals in combination with the LYP correlation functional taking the QM region as R1 and the basis sets as B1L, B2L, and B2W. Since we are primarily interested in the intrinsic preference of a functional with a different HF admixture on the relative state energies, we have chosen to calculate single-point energies on the B3LYP-optimized geometry of the corresponding spin state at the R1/B1L level instead of optimizing at each level. The results are given in Figures 2 and 3 for the ferric and ferrous complexes, respectively.

In the gas phase, the pure density functional BLYP exhibits a clear preference for the doublet state of the *ferric complex* as the ground state and gives the energy sequence as doublet < quartet < sextet with all basis sets (see Figure 2a). On the other hand, the BHLYP functional with 50% exact exchange favors the sextet state strongly as the ground state and predicts the energy ordering of the spin states as sextet < quartet < doublet with all basis sets. We have already discussed in section III.A that the state sequences obtained with B3LYP depend on the chosen basis set: the preferred B2W basis set yields sextet < quartet < doublet.

When moving from the gas phase to the protein environment (see the QM energies given in Figure 2a,b), the quartet state is stabilized by ca. 9 kcal/mol at the BHLYP/B2W level and by 3 kcal/mol at all the remaining levels while the doublet state is generally destabilized by ca. 3−4 kcal/mol. Consequently, the BLYP (B3LYP) {BHLYP} state ordering of QM energies in the protein environment becomes quartet < doublet < sextet

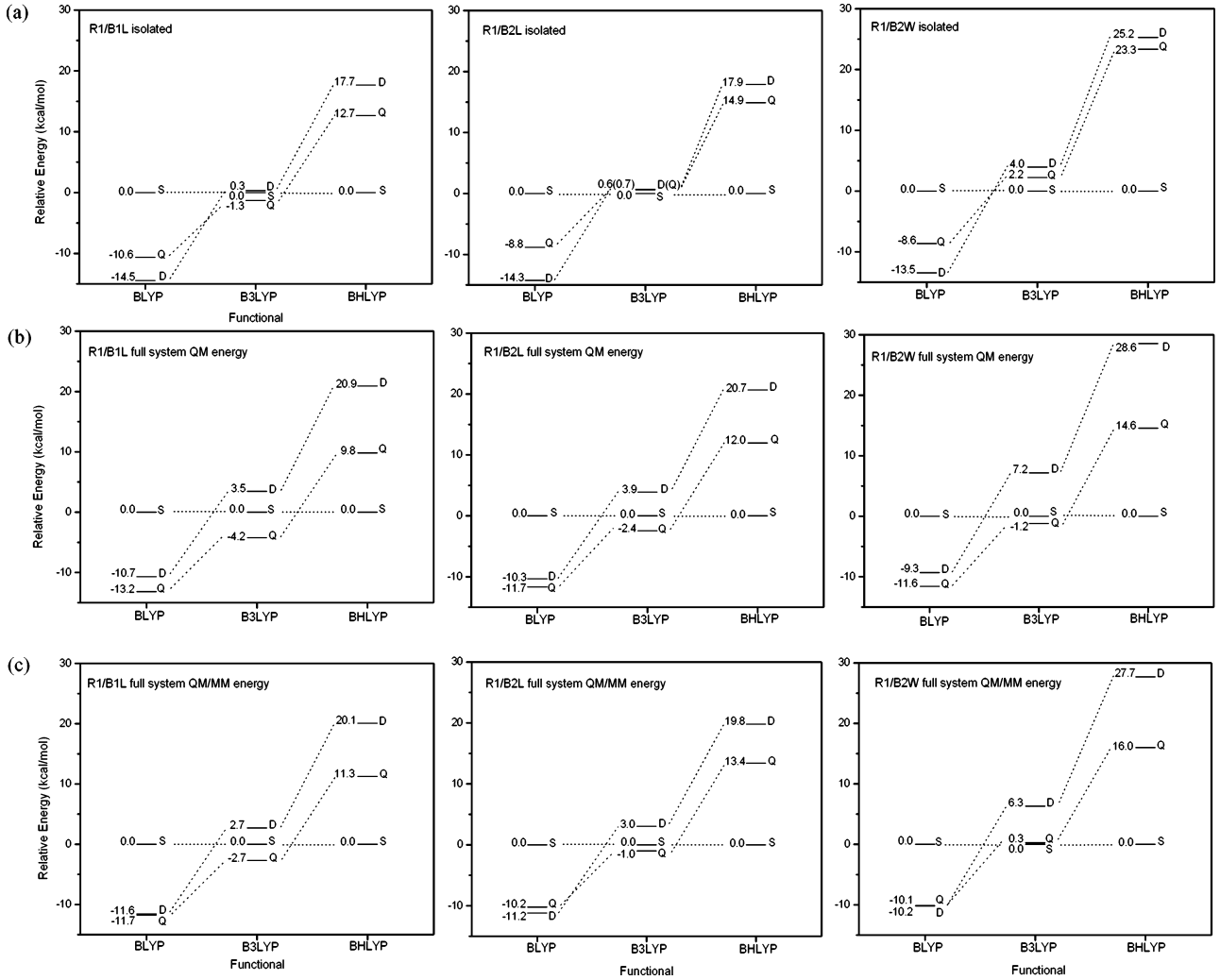

Figure 2. The influence of exact exchange on the relative energies (kcal/mol) of doublet (D) and quartet (Q) states with respect to the sextet (S) state of the pentacoordinated ferric $P450_{cam}$ complex (snapshot 93) computed on the B3LYP optimized geometries at the R1/B1L level: (a) the isolated system QM energy differences; (b) QM/MM system QM energy differences; and (c) QM/MM energy differences.

(quartet < sextet < doublet) {sextet < quartet < doublet} with all basis sets considered.

When the MM contributions are also included to yield QM/MM energies (see Figure 2b,c), the quartet (doublet) state is destabilized (stabilized) by ca. 1.5 kcal/mol (ca. 1 kcal/mol) compared to the sextet state for all functionals and basis sets. Note that this is the inverse trend of the corresponding QM contributions (see above). The destabilizing effect of the MM contributions on the energy of the quartet makes the sextet slightly favored at the B3LYP/B2W level.

The overall effect of the protein environment (see Figure 2a,c) is a stabilization of the quartet state with respect to the sextet state by ca. 7 kcal/mol for the BHLYP/B2W level and by ca. 1−2 kcal/mol for all the remaining cases, and a destabilization of the doublet state by ca. 2−3 kcal/mol. An increasing amount of HF exchange included in the functional always has a destabilizing effect on the quartet and doublet states.

For the *ferrous complex*, the state ordering is the same for all basis sets used in this study. The inclusion of exact exchange causes a destabilization of singlet and triplet states relative to the quintet state, and the amount of destabilization again appears to be directly proportional to the amount of HF admixture.

In the gas phase, the pure density functional BLYP prefers the singlet structure as the ground state and gives the order singlet < triplet < quintet (see Figure 3a). The admixture of HF exchange in B3LYP and BHLYP inverts this sequence to quintet < triplet < singlet.

Going from the gas phase to the protein environment (see the QM energies given in Figure 3a,b), the triplet (singlet) state is stabilized (destabilized). MM contributions to QM energies generally stabilize (destabilize) the singlet (triplet) state by ca. 1.9 kcal/mol (ca. 2.2 kcal/mol) (see Figure 3b,c). Overall, BLYP gives a singlet ground state in the gas phase and a triplet ground state in the presence of protein environment, whereas B3LYP and BHLYP always favor a quintet ground state (quintet < triplet < singlet).

The dependence of the relative energies of HS, IS, and LS states on the fraction of HF exchange in the density functional has previously been discussed for hexacoordinated Fe(II)−sulfur complexes,[21] the resting form of P450 in gas-phase models[22] and in the protein environment,[20] and imidazole ligated penta- and hexacoordinated heme complexes.[23] In the gas phase, pure density functionals favor IS for the imidazole ligated ferrous pentacoordinated heme complex according to previous work,[23,50] and LS for the pentacoordinated heme−SH complex according to our present BLYP results. Thus, the nature of the proximal ligand can influence the propensity for a given spin state. The B3LYP and BHLYP functionals with an all-electron basis set give the energy sequence HS < IS < LS and thus correctly

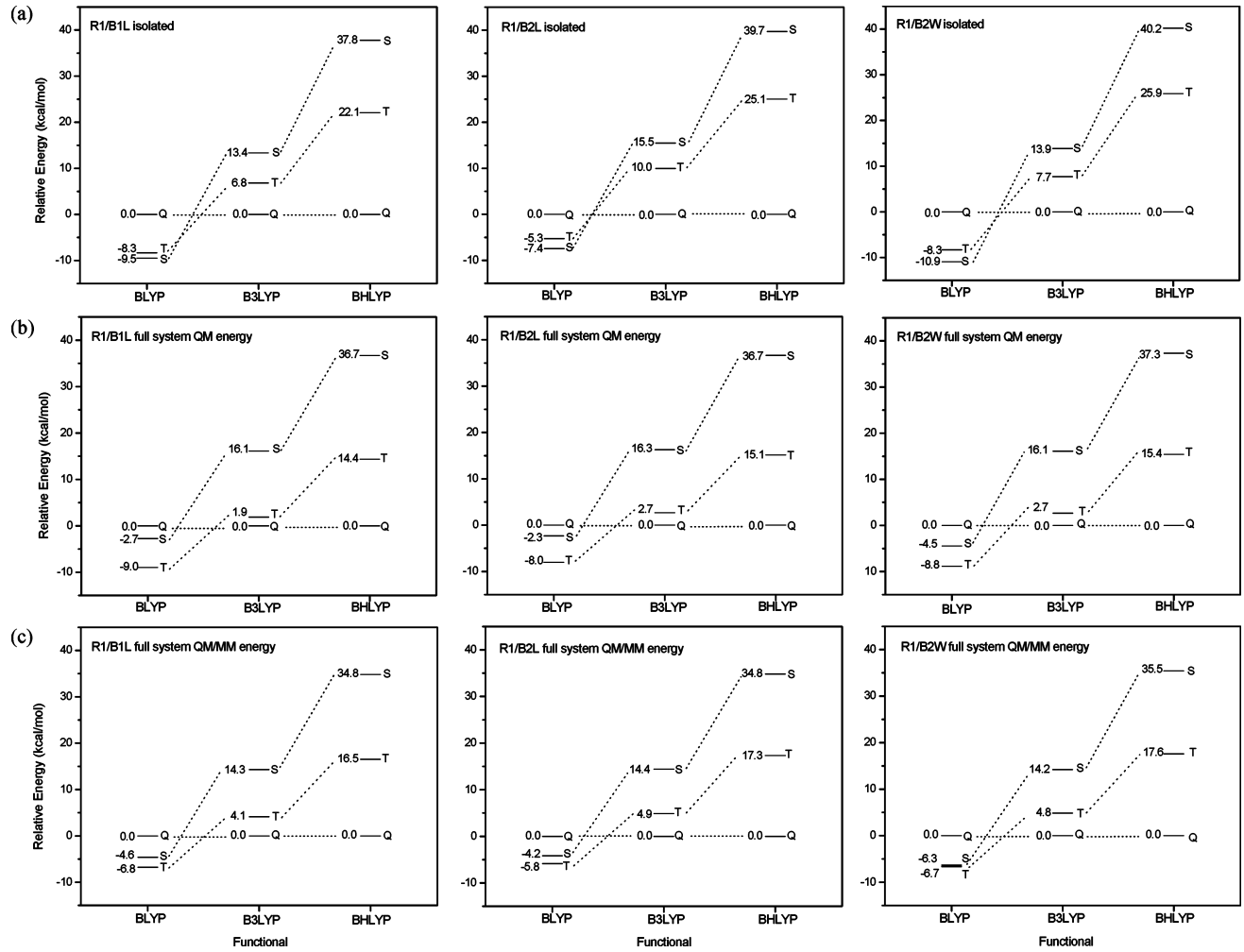

Figure 3. The influence of exact exchange on the relative energies (kcal/mol) of singlet (S) and triplet (T) states with respect to the quintet (Q) state of the pentacoordinated ferrous $P450_{cam}$ complex (snapshot 93) computed on the B3LYP optimized geometries at the R1/B1L level: (a) the isolated system QM energy differences; (b) QM/MM system QM energy differences; and (c) QM/MM energy differences.

TABLE 2: Relative Energies (kcal/mol) of the Quartet and Doublet States of the Ferric Complex (QM Regions: R1 and R2) with Respect to the Sextet State Computed with Basis Sets B1L/B2L/B2W

		$E(^4A) - E(^6A)$		$E(^2A) - E(^6A)$	
snapshot	ΔE^a	R1	R2	R1	R2
31	$\Delta E^{QM/MM}$(p,p)	−2.5/−0.7/0.6	−2.5/−0.5/1.0	3.4/3.7/6.7	2.3/2.2/5.0
	ΔE^{QM}(p,p)	−4.0/−2.5/−1.1	−4.2/−2.2/−0.7	3.9/4.3/7.3	2.0/2.0/4.8
	ΔE^{QM}(p,g)	−1.2/0.8/2.4	−1.5/0.8/2.4	2.2/2.4/5.4	0.4/0.6/3.2
	ΔE^{QM}(g,g)	−1.3/0.9/2.4	−2.7/−0.4/1.0	0.3/0.6/3.8	−0.2/0.0/3.0
93	$\Delta E^{QM/MM}$(p,p)	−2.7/−0.9/0.5	−2.7/−0.6/0.7	2.7/3.1/6.1	1.5/1.6/4.4
	ΔE^{QM}(p,p)	−4.2/−2.4/−1.1	−4.2/−2.0/−0.9	3.5/3.7/6.6	1.6/1.7/4.5
	ΔE^{QM}(p,g)	−1.2/1.1/2.6	−1.7/0.8/2.2	2.2/2.5/5.4	0.2/0.3/3.0
	ΔE^{QM}(g,g)	−1.3/0.9/2.4	−2.7/0.0/1.1	0.3/0.6/3.8	−0.2/0.4/2.4

[a] ΔE energy differences from top to bottom in the column correspond to QM/MM (B3LYP/CHARMM) energy difference, QM (B3LYP) contribution to QM/MM energy, energy difference of the naked system at the protein geometry, and energy difference of the naked system at the gas-phase geometry. A positive (negative) ΔE value implies that the reference state ^6A has lower (higher) energy.

predict the experimental HS ground-state nature of the pentacoordinated complexes.

The HS state is systematically favored in HF-type theories since Fermi correlation is incorporated in the wave function, while Coulomb correlation is not.[51] Reiher et al.[21] suggested using a HF exchange ratio of 15% in the density functional (dubbed B3LYP*) for better quantitative predictions of the HS−LS gap in hexacoordinated ferrous complexes. However, since reasonably accurate results have been obtained with B3LYP for many systems,[52] we prefer in the following to utilize the standard B3LYP functional, which has an exact exchange admixture of 20% (close to B3LYP*). The BHLYP functional obviously exaggerates the sextet−doublet gap significantly, considering the experimentally observed spin equilibrium.

C. The Influence of Protein Environment. *1. Relative Energies.* The energies of quartet and doublet states of the *ferric complex* with respect to the sextet state in the presence and absence of protein environment are given in Table 2 for both snapshots (QM regions: R1 and R2; basis sets: B1L, B2L, and B2W; functional: B3LYP).[53] The results obtained for both snapshots are almost identical with typical deviations in relative energies of 0.3 kcal/mol or less. The results for different QM

TABLE 3: Adiabatic [$E(S_{g,g}) - E(S_{p,p})$] and Vertical [$E(S_{p,g}) - E(S_{p,p})$] QM (B3LYP) Energy Differences (kcal/mol) of the $^6A/^4A/^2A$ State Ferric Pentacoordinated $P450_{cam}$ Complex

		$E(S_{g,g}) - E(S_{p,p})$		$E(S_{p,g}) - E(S_{p,p})$	
snapshot		R1	R2	R1	R2
31	B1L[a]	94.8/97.6/91.2	121.7/123.2/119.5	101.7/104.5/100.0	140.7/143.3/139.1
	B2L	94.2/97.6/90.5	122.6/ 124.4/120.6	101.6/104.9/99.8	140.1/143.1/138.7
	B2W	94.0/97.5/90.5	122.2/124.0/120.5	101.4/104.9/99.5	140.0/139.1/138.4
93	B1L	91.8/94.7/88.6	124.9/126.5 /123.1	98.8/101.8/97.5	144.3/146.9/ 143.0
	B2L	91.7/94.9/88.5	125.5/ 127.5/124.2	99.1/102.5/97.8	143.6/ 146.4/142.3
	B2W	91.4/94.9/88.6	125.4/127.4/123.4	99.8/102.5/97.6	143.5/146.5/142.0

[a] R1/B1L results for protonation state Prot2 with zero net charge: adiabatic 99.2/101.8/94.7, vertical 105.9/108.9/103.5

TABLE 4: Relative Energies (kcal/mol) of the Triplet and Singlet States of the Ferrous Complex (QM Regions: R1 and R2) with Respect to the Quintet State Computed with Basis Sets B1L/B2L/B2W

		$E(^3A) - E(^5A)$		$E(^1A) - E(^5A)$	
snapshot	ΔE[a]	R1	R2	R1	R2
31	$\Delta E^{QM/MM}(p,p)$	4.4/5.6/5.2	4.1/5.6/5.0	15.3/15.9/15.2	14.4/14.4/13.9
	$\Delta E^{QM}(p,p)$	2.7/2.9/1.9	2.4/4.0/3.4	17.3/16.2/15.4	15.1/14.6/14.6
	$\Delta E^{QM}(p,g)$	6.4/10.4/9.3	5.1/7.1/6.3	12.8/15.8/14.0	10.9/10.8/10.9
	$\Delta E^{QM}(g,g)$	6.8/10.1/7.5	3.1/6.7/5.0	13.4/15.5/13.9	11.9/13.6/12.1
93	$\Delta E^{QM/MM}(p,p)$	4.1/5.6/5.1	3.3/5.0/5.4	14.3/15.0/14.3	12.7/13.1/13.2
	$\Delta E^{QM}(p,p)$	1.9/3.4/1.4	1.2/2.5/2.2	16.1/16.0/14.6	14.1/13.9/13.4
	$\Delta E^{QM}(p,g)$	6.0/10.2/8.1	5.1/7.0/6.3	12.4/15.5/13.6	10.2/10.5/10.2
	$\Delta E^{QM}(g,g)$	6.8/10.1/7.5	3.1/6.7/4.9	13.4/15.5/13.9	11.9/13.6/12.1

[a] ΔE energy differences from top to bottom in the column correspond to QM/MM (B3LYP/CHARMM) energy difference, energy difference between QM (B3LYP) contributions to QM/MM energy, energy difference of the naked system at the protein geometry, and energy difference of the naked system for the gas-phase geometry. A positive (negative) ΔE value implies that the reference state ^5A has lower (higher) energy.

regions (R1, R2) in the presence of the protein environment are rather similar for the quartet−sextet gap (usually within 0.4 kcal/mol) whereas the differences are more pronounced in the case of the doublet−sextet gap (typically lower by 1−2 kcal/mol for R2 compared with R1). Still larger variations in the computed relative energies are caused by the choice of basis set: extension of the basis leads to a differential stabilization of the sextet state, by around 3−5 kcal/mol when comparing the smallest (B1L) and largest (B2W) set, and may cause a change in the state sequence (e.g., quartet vs sextet).

Focusing on the best available B3LYP results obtained at the R2/B2W level, the sextet is found to be the ground state in the enzyme, in accord with experiment. However, the quartet is only slightly higher in energy, by about 1 kcal/mol, both in the enzyme and in the gas phase; the MM contributions to the QM/MM energy favor the sextet over the quartet, whereas the QM/MM electrostatic interactions exert an opposing influence (see Table 2). The doublet is computed to be 4−5 kcal/mol above the sextet in the enzyme (R2/B2W), with a differential destabilization by the enzyme environment of about 2 kcal/mol relative to the gas-phase situation (see Table 2).

Experimentally, the sextet ground state is known to be in equilibrium with the doublet state, which must thus be very close energetically. Hence, our best B3LYP calculations overestimate the doublet−sextet gap. In view of the strong dependence on the amount of HF exchange included in the hybrid functional (see section III.B), this is not too surprising. Single-point calculations (R2/B2W) on snapshot 31 with the recommended[21] admixture of 15% HF exchange with ORCA bring the quartet−sextet and the doublet−sextet gaps to 0.6 and −1.6 kcal/mol, respectively, resulting in a doublet ground state. More accurate correlated ab initio methods are evidently needed for more reliable predictions of the relative spin state energies.

Adiabatic and vertical QM energies of each state of the *ferric complex* are given in Table 3 to assess the influence of protein environment further. The results are essentially the same for all basis sets considered. The vertical energies at the geometry of the protein measure the stabilization of the QM region through electrostatic interactions with the protein environment, which is larger for the larger QM region (ca. 100 kcal/mol for R1 and ca. 140 kcal/mol for R2). The substantial differences between vertical and adiabatic energies (ca. 8 kcal/mol for R1 and 20 kcal/mol for R2) arise from the energy change due to the relaxation in the gas phase, indicating that the *ferric complex* is strained in the protein pocket (more so for the larger R2 model with a more extended proximal ligand, see Figure 1).

In the case of the *ferrous complex*, we have obtained two closely lying quintet minima with different orbital occupations, i.e., with a doubly filled $d_{x^2-y^2}$ (electromer **a**) or d_{xz} (electromer **b**) orbital. The QM/MM calculations with QM region R2 favor electromer **b** with all basis sets by ca. 0.5 kcal/mol. However, the QM/MM calculations with QM region R1 do not present any clear preference for the electromers. In gas-phase optimizations, electromer **a** is more stable than electromer **b** by ca. 2 kcal/mol. The results given in the following always refer to the lowest energy electromer obtained. However, the geometry parameters and spin densities of the two electromers are very similar to each other. The Fe−S bond in electromer **b** is slightly weaker.

Table 4 lists the energies of triplet and singlet states of the *ferrous complex* with respect to the quintet state for two snapshots in the presence and absence of protein environment (QM regions: R1 and R2; basis sets: B1L, B2L, and B2W; functional: B3LYP). For both snapshots, the energy ordering is quintet < triplet < singlet in all cases. The quintet lies 3−6 kcal/mol (13−16 kcal/mol) lower in energy than the triplet (singlet) in the protein environment. Compared with the gas phase, there are only rather minor changes in relative stabilities (typically 2 kcal/mol or less).

Adiabatic and vertical QM energies of each state of the *ferrous complex* are listed in Table 5. These energies are much lower than those for the *ferric complex* (Table 3) for Prot1. In the case of the *ferrous complex*, the QM region has a net charge of −1e due to the uptake of one electron while the MM region

TABLE 5: Adiabatic [$E(S_{g,g}) - E(S_{p,p})$] and Vertical [$E(S_{p,g}) - E(S_{p,p})$] B3LYP QM Energy Differences (kcal/mol) of the $^5A/^3A/^1A$ State Ferrous Pentacoordinated P450$_{cam}$ Complex

		$E(S_{g,g}) - E(S_{p,p})$		$E(S_{p,g}) - E(S_{p,p})$	
snapshot		R1	R2	R1	R2
31	B1L[a]	2.5/6.6/−1.5	25.1/25.8/21.8	10.8/14.5/6.3	43.9/46.6/39.6
	B2L	0.4/7.6/−0.3	24.4/27.1/23.4	8.1/15.6/7.6	43.7/46.7/39.9
	B2W	0.3/5.9/−1.2	24.6/26.2/22.1	8.1/15.5/6.7	42.7/45.6/39.0
93	B1L	6.4/11.3/3.6	35.4/37.3/33.3	15.0/19.1/11.3	55.2/59.0/51.3
	B2L	5.2/11.9/4.7	35.3/39.5/35.0	13.0/19.8/12.5	55.1/59.7/51.8
	B2W	4.6/10.7/3.9	35.5/38.2/34.2	12.7/19.4/11.7	54.1/58.2/50.9

[a] R1/B1L results for protonation state Prot2 with zero net MM charge: adiabatic 142.6/147.6/137.6, vertical 150.7/155.8/145.7

in Prot1 has a net charge of −9e (surface charges on the enzyme that are screened by the solvent, but not compensated by counterions). The stabilization due to the polarization of the QM region by the electric field of the protein environment is thus counteracted by the destabilization due to long-range electrostatic interactions between the net charges in the QM and MM regions. The latter is missing in the *ferric complex* with a neutral QM region, which explains the discrepancies between the results in Tables 3 and 5. On the other hand, the differences between the vertical and adiabatic QM energies are almost the same in Tables 3 and 5, indicating similar relaxation energies of the QM region in the gas phase, and hence similar strain of the ferric and ferrous complexes in the enzyme.

The preceding interpretation is confirmed by test calculations for protonation state Prot2 with zero net charge (neutralized, see section II.B). B3LYP/CHARMM geometry optimizations at the R1/B1L level for the entire ferric {ferrous} Prot2 system (snapshot 31) yield (IS−HS)/(LS−HS) QM/MM energy differences of −2.5/4.2 {4.3/16.9} kcal/mol, which are quite close to the values of −2.5/3.4 {4.4/15.3} kcal/mol for protonation state Prot1 (see Tables 2 and 4). Likewise, the corresponding R1/B2W single-point results at the R1/B1L optimized geometries are similar to each other: 0.2/7.7 {4.2/16.6} kcal/mol for Prot2 and 0.3/6.3 {4.8/14.2} kcal/mol for Prot1 (see Figures 2 and 3). Hence, the neutralization of distant residues in Prot2 has only a very minor influence on the relative spin state energies, and also on the computed stabilization energies for the *ferric complex* with a zero net charge in the QM region (see Table 3). On the other hand, as expected, it strongly affects the stabilization energies for the *ferrous complex* with a −1e net charge in the QM region (see Table 5), by avoiding artificial long-range electrostatic interactions.

The reduction potential ϵ for the one-electron process $\mathbf{2} + e^- \rightarrow \mathbf{3}$ is determined by the corresponding free energy change $\Delta G = -F\epsilon$ where $F = 23.062$ kcal/(mol·V) is the Faraday constant. Approximating ΔG by the energy change $\Delta E = E(\mathbf{3},^5A) - E(\mathbf{2},^6A)$ and using the potential of the standard hydrogen electrode as reference ($\epsilon^\circ_{ref} = -4.43$ V),[54] the absolute one-electron reduction potential ϵ° is obtained from the formula $\epsilon^\circ = \epsilon^\circ_{ref} - \Delta E/F$. The computed (R1/B1L, B3LYP) reaction energies ΔE and reduction potentials ϵ° for Prot1/Prot2/(gas phase) are 53.81/−81.61/−46.77 kcal/mol and −6.76/−0.89/−2.40 V, respectively. Obviously, Prot1 is not adequate for estimating the experimental reduction potential of reductase-free *ferric complex* (−170 mV) due to long-range electrostatic interactions between the net QM (−1e) and MM (−9e) charges in the *ferrous complex* that disfavor the reaction artificially as explained above and make it endothermic. The reduction is computed to be exothermic in the gas phase and the neutral MM environment (Prot2), significantly more so in the latter case: the electric field of the MM environment favors the reduced form by ca. 35 kcal/mol relative to the gas phase. The computed reduction potentials of −2.40 (gas phase) and −0.89 V (Prot2) compare well with recently published DFT values[19] of −2.82 (gas phase) and −0.95 V (medium with a dielectric constant of 80). The best present results (Prot2) still differ from the experimental reduction potential (−0.17 V) by 0.72 V implying that the electron affinity ($-\Delta E$) of the *ferric complex* is underestimated by ca. 17 kcal/mol. To put this discrepancy into perspective one should first note the intrinsic accuracy of DFT for electron affinities. While it is known that DFT is capable of yielding reasonable electron affinities for larger molecules even with moderate basis sets,[55] it is also generally accepted that basis sets of at least triple-ζ quality augmented with diffuse functions are needed to obtain converged results.[56,57] For example, the B3LYP electron affinity of bacteriopheophytin, a free-base porphyrin-like chromophore, increases by ca. 9 kcal/mol when going from 6-31G or 6-31G** to the larger cc-pVTZ(-f)++ basis, and the resulting best values still deviate from experiment.[55] Given the intrinsic limitations of the current DFT calculations, errors of the order of 10 kcal/mol in the computed electron affinity of the *ferric complex* would not be surprising.

A potentially even more serious problem is the lack of configurational sampling. Recent free energy calculations on reduction potentials in enzymes[58,59] have emphasized the importance of proper configurational sampling and the need for a complete representation of the protein and solvent environment. The QM/MM work on the first reduction potential of flavin adenine dinucleotide (FAD) in cholesterol oxidase has shown,[59] for example, that the intra-FAD reorganization energy upon reduction is relatively small (ca. 5 kcal/mol) while the reorganization energy of the protein is rather large (−39 kcal/mol) and partly counterbalanced by the reorganization in the bulk solvent (+26 kcal/mol). Our approach with separate QM/MM geometry optimizations for the *ferric* and *ferrous* complexes will capture some of the structural reorganization, but only for a selected snapshot, and it is unclear how much this will deviate from a properly averaged value, in view of the observed fluctuations.[58,59] It seems fair to note, however, that the computation of reduction potentials in enzymes is generally a challenging problem and that there are also substantial deviations between available free energy results[58,59] and the corresponding experimental data.

2. Spin Densities. The spin densities obtained from B3LYP/CHARMM calculations for the snapshots 31 and 93 and from B3LYP calculations for the isolated gas-phase systems are documented in Tables S1 and S2 of the Supporting Information for the ferric and ferrous complexes, respectively. For each QM region (R1 and R2) and basis set (B1L, B2L, and B2W), data are given for the full system (QM/MM optimized), the isolated gas-phase model at the protein geometry (QM), and the isolated optimized gas-phase model (QM). The results are quite similar for both snapshots and both QM regions, and there is only a minor basis set dependence. Therefore, we present in Tables 6 and 7 only some selected spin densities obtained for snapshot

TABLE 6: Spin Densities of ^{6}A, ^{4}A, and ^{2}A States of the Ferric Pentacoordinated P450$_{cam}$ Complex Computed for the B3LYP/CHARMM-Optimized Structure ($S_{p,p}$)/the Isolated QM System in Its Protein Geometry ($S_{p,g}$)/the Isolated QM System in Its Gas-Phase Geometry ($S_{g,g}$): Snapshot 31, R2/B2W Level

	^{6}A	^{4}A	^{2}A
Fe[a]	4.015/3.990/4.006	2.583/2.482/2.535	1.198/1.151/1.142
SL[b]	0.383/0.507/0.441	0.375/0.499/0.425	−0.049/−0.027/−0.029
Porp[b]	0.601/0.503/0.553	0.042/0.019/0.040	−0.149/−0.123/−0.114

[a] Atomic spin density. [b] Group spin density, which is the sum of spin densities on each atom within the porphyrin (Porp) cycle or the proximal ligand (SL) of QM region R2.

TABLE 7: Spin Densities of ^{5}A and ^{3}A States of the Ferrous Pentacoordinated P450$_{cam}$ Complex Computed for the QM/MM-Optimized Structure ($S_{p,p}$)/the Isolated QM System in Its Protein Geometry ($S_{p,g}$)/the Isolated QM System in Its Gas-Phase Geometry ($S_{g,g}$): Snapshot 31, R2/B2W Level[a]

	^{5}A	^{3}A
Fe[b]	3.706/3.703/3.644	1.988/1.945/1.973
SL[c]	0.132/0.193/0.139	0.109/0.194/0.161
Porp[c]	0.162/0.104/0.217	−0.098/−0.138/−0.134

[a] As the singlet is a closed-shell system, the spin density on each atom is zero. [b] Atomic spin density. [c] Group spin density, which is the sum of spin densities on each atom within the porphyrin (Porp) cycle or the proximal ligand (SL) of QM region R2.

SCHEME 3

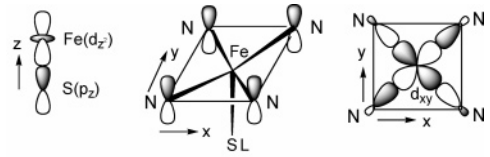

31 at the preferred R2/B2W level, and concentrate on these results in our discussion.

In the *ferric complex*, the unpaired spin of the doublet state is largely localized on the iron atom. The excess of α spin on iron arises mainly from the interaction of the d_{z^2} orbital of iron with the sulfur p_z (see Scheme 3a) and a_{2u}-porphyrin (see Scheme 3b, which shows only the nitrogen p_z orbitals for simplicity) orbitals. These interactions yield an anionic radical character for the porphyrin ring and the proximal ligand. When moving from the structure optimized in the gas phase to the protein environment, the excess spin density on each atom increases slightly.

In the quartet state, the iron d_{z^2} orbital interacts with the sulfur p_z orbital (antibonding σ^* interaction shown in Scheme 3a) such that the proximal ligand acquires some cationic radical character (0.3−0.5 e). The porphyrin moiety does not carry much spin density. In the protein environment, the spin density at sulfur is lower than that in the gas phase, indicating an increased electron density at sulfur due to favorable electrostatic interactions with neighboring residues.

In the sextet state, the iron d_{xy} orbital mixes with sp^2 orbitals of the pyrrole nitrogens (antibonding σ^* interaction shown in Scheme 3c). As a result, one unpaired electron is delocalized over the porphyrin macrocycle (0.6 e in the protein pocket, mainly at pyrrole nitrogens, and 0.5 e in the gas phase) and the proximal ligand (0.4−0.5 e). The spin density distribution on the proximal ligand is almost identical in the quartet and sextet states. When going from the gas phase to the protein environment, notable changes of the order of 0.1 e occur in the spin densities of porphyrin and sulfur (see Table 7).

The singlet state of the *ferrous complex* is a closed-shell system, and thus there is no net spin on any atom. In the triplet state, the iron orbitals couple only weakly with the nitrogen and sulfur orbitals. Hence, the two unpaired electrons in the triplet state are primarily localized in iron d_{yz} and d_{z^2} orbitals. The excess α (β) spin density on sulfur (porphyrin) decreases slightly when moving to the protein environment. In the quintet state, the iron d_{xy} orbital mixes with sp^2 orbitals of the pyrrole nitrogens as in the sextet state of the *ferric complex* (see Scheme 3c), which results in a transfer of 0.1−0.2 e to porphyrin. The computed localization of the added electron mainly at the iron is in agreement with the Mössbauer spectrum[7] of the ferrous complex.

The positive spin density at the sulfur ligand is generally reduced when going from the gas phase to the protein pocket. This implies that sulfur gains some electron density (acquiring more closed-shell character), which suggests that the polarizing medium of the protein environment stabilizes electron density on sulfur. When the individual average spin densities of the atoms on the porphyrin ring (see Tables S1 and S2 of the Supporting Information) are compared to each other for each spin state, it is seen that the excess α or β spin densities are dominantly located on pyrrole nitrogens, with lesser contributions from meso carbons. This indicates that the unpaired spin densities of the porphyrin arise from an a_{2u}-like orbital.

3. Geometries. Table 8 compares the H-bond distances in the snapshots (before and after QM/MM optimizations) with those in the X-ray structures (PDB codes: 1DZ4, 2CPP, 1DZ6).[11,24] The missing H-positions in the X-ray structures were determined by CHARMM optimizations keeping the heavy atoms fixed. The H-bonds seen around the reactive center in the X-ray structures are present in both snapshots, which thus provide realistic descriptions of the protein environment. The deviation of ca. 0.2 Å between computed and experimental H-bond distances can be attributed partly to the experimental uncertainty of 0.2 Å in the Fe−S bond, and partly to the limited accuracy of the adopted force field parameters, in particular the van der Waals parameters that describe QM/MM interactions (see ref 60 and references therein). During the QM/MM geometry optimizations, the H-bond distances are generally reduced significantly from their initial values (obtained from a classical MD trajectory). In the gas phase, the amino hydrogen of Leu358 does not form a H-bond with the nitrogen atom of the D pyrrole, leading to a reorientation of Leu358.

Geometrical parameters around the iron center of the ferric and ferrous complexes calculated both in the presence (B3LYP/CHARMM) and absence (B3LYP) of the enzyme environment are given in Tables S3 and S4 of the Supporting Information, for snapshots 31 and 93, respectively, together with the available X-ray data. These tables document the theoretical results for both QM regions (R1, R2) and all basis sets (B1L, B2L, B2W) employed. The computed trends in the geometrical parameters are the same in both snapshots and for both QM regions, and the results are not too sensitive to the choice of the basis set (except for the Fe−S bond lengths which shorten significantly upon basis set extension). Therefore, we present in Table 9 only some selected geometrical data for snapshot 31 obtained at the preferred R2/B2W level.

In both complexes, iron generally tends to form the shortest bonds in the LS species. However, the difference between computed Fe−N distances of the LS and IS states is often small. As the sixth coordination site of iron is empty, iron is attracted by and displaced toward the sulfur ligand. The HS states have an antibonding Fe(d_{xy})−N(sp^2) σ^* molecular orbital (MO) (see

TABLE 8: XH···Y Hydrogen Bond Distances around the Reactive Center, Given as X−Y (H−Y), Where X = N, O and Y = S, N, O, for R2/B2W-Optimized Snapshots and X-ray Structures (H-Positions from CHARMM Optimizations with Fixed Heavy Atoms)

		Leu358−Cys357 NH···S	Leu358−Heme NH···N_D	Gly359−Cys357 NH···S	Gln360−Cys357 NH[a]···S	Gln360−Cys357 NH[b]···O=C	Tyr96−Camphor OH···O
^{6}A	1DZ4 + H	3.53 (3.65)	4.07 (3.30)	3.30 (2.52)	3.27 (3.07)	2.97 (1.99)	2.72 (1.78)
	2CPP + H	3.57 (3.73)	4.28 (3.59)	3.25 (2.53)	3.40 (3.39)	3.08 (2.57)	2.65 (1.72)
	snapshot 31	3.37 (3.30)	4.09 (3.16)	3.33 (2.53)	3.77 (3.42)	2.93 (1.92)	2.79 (1.82)
	snapshot 93	3.42 (3.42)	4.05 (3.16)	3.49 (2.92)	3.74 (3.59)	2.86 (1.86)	2.76 (1.79)
^{5}A	1DZ6 + H	3.51 (3.72)	3.82 (3.08)	3.15 (2.37)	3.24 (2.94)	3.03 (2.04)	2.69 (1.77)
	snapshot 31	3.31 (3.10)	3.95 (2.96)	3.23 (2.38)	3.53 (2.90)	2.94 (1.94)	2.77 (1.81)
	snapshot 93	3.37 (3.25)	3.97 (3.01)	3.33 (2.63)	3.51 (3.07)	2.84 (1.84)	2.76 (1.81)
before QM/MM	snapshot 31	3.57 (3.76)	4.11 (3.42)	3.44 (2.95)	3.79 (3.68)	3.00 (2.01)	2.77 (1.82)
optimization	snapshot 93	3.62 (3.79)	4.14 (3.44)	3.73 (3.41)	3.80 (3.85)	2.88 (1.88)	2.77 (1.82)

[a] Backbone. [b] Side chain.

TABLE 9: Computed and Experimental Geometry Parameters (Bond Length *r* and Out-Of-Plane Distance d_δ in Å) of Each State of the Pentacoordinated Ferric and Ferrous Complexes around the Iron Center: Snapshot 31, R2/B2W Level

	ferric complex (^{6}A/^{4}A/^{2}A)		ferrous complex (^{5}A/^{3}A/^{1}A)	
	QM/MM[a]	gas phase[b]	QM/MM[a]	gas phase[b]
r(Fe−S)	2.349/2.413/2.228	2.330/2.405/2.210	2.460/2.623/2.320	2.440/2.521/2.309
r_{av}(Fe−N)	2.102/2.035/2.028	2.099/2.022/2.011	2.128/2.047/2.038	2.145/2.032/2.018
d_δ	0.44/0.27/0.24	0.48/0.29/0.24	0.41/0.20/0.19	0.59/0.23/0.18

[a] B3LYP/CHARMM QM/MM geometry optimization. [b] B3LYP QM optimization of the isolated QM subsystem R2.

Scheme 3c), and therefore the Fe−N bond length and the out-of-plane distance d_δ between the iron atom and the average plane of pyrrole nitrogens are larger in the HS states than in the corresponding LS and IS states. The Fe−N distances in the heme moiety exhibit small differences of 0.00−0.03 Å, and thus only the average value is given in Table 9. When moving from the gas phase to the protein pocket, there is no clear trend for the change in the individual Fe−N distances. The notable discrepancies between two experimental data (PDB codes: 1DZ4 and 2CPP) for the Fe−N bond lengths of the *ferric complex* impede a comparison with the computed bond lengths.

The iron out-of-plane distance d_δ depends on the spin multiplicity. The relative stability of different spin states can be influenced by small changes in d_δ. We have investigated this further as follows: starting from the optimized geometry of each state (R1/B2W), the iron atom was moved along the Fe−S bond, constraining the N_A−Fe−N_C and N_B−Fe−N_D angles to fix d_δ and optimizing all other degrees of freedom. The resulting energy profiles are depicted in Figures 4 and 5 for the ferric and ferrous complexes, respectively. The sextet state is destabilized significantly when iron is moved toward the protoporphyrin IX plane. It crosses the quartet and doublet states in the gas phase (at 0.31 and 0.25 Å), but only the quartet state in the protein environment (at 0.33 Å). This emphasizes again that the three spin states are energetically close in the *ferric complex* (see above): moderate out-of-plane motions can change their energetic sequence (Figure 4). By contrast, we do not find such crossings in the *ferrous complex* where the quintet state remains the ground state at all geometries considered (Figure 5).

The Fe−S bond is generally longer in the HS and IS states than in the LS state (see Table 9) because of the population of the iron d_{z^2} orbital, and hence the Fe−S σ* MO (see Schemes 2 and 3a). The Fe−S bond, which shortens with the basis set improvement, is generally found to be stronger in the gas phase than in the protein pocket, especially in the case of the *ferrous complex*. As the experimental uncertainty for the Fe−S bond is large (0.2 Å), a conclusive comparison between theory and experiment is again impossible. Comparing the HS and IS states, the iron out-of-plane distance d_δ is typically twice as large in the HS state, with a concomitant significant shortening of the Fe−S bond (see Table 9). This correlation is depicted in Figure 6, which shows the response of the Fe−S bond length to moderate changes in the iron out-of-plane distance, for all spin states of the ferric and ferrous complexes. It may be rationalized by noting that, for increasing out-of-plane distances, the iron d_{z^2} orbital can interact more strongly with the distal lobe of the porphyrin a_{2u} orbital, which will tend to diminish the antibonding character of the corresponding Fe−S σ* MO (see Scheme 3a,-3b).

D. Mössbauer Parameters. The computed and experimental[6,7,61] Mössbauer parameters of the ferric and ferrous complexes are given in Table 10 for each spin state. QM/MM results for the enzyme ($S_{p,p}$) are compared with QM results for gas phase ($S_{g,g}$) to probe if the latter can represent the real system. There is generally reasonable agreement between these two sets of theoretical results for the isomer shifts, but there are sometimes considerable deviations in the computed quadrupole splittings and asymmetry parameters so that a full QM/MM treatment would seem preferable in the latter case.

In the *ferric complex*, the calculated isomer shifts for all spin states are close to each other and to the experimental value. Larger discrepancies are found for the quadrupole splitting: the computed value for the sextet best matches the experimental value for the ground state (known to be a sextet) but the deviation of 0.4 mm/s is quite sizable. The experimental asymmetry parameter is, however, reasonably well reproduced by the calculated value for the sextet state.

The *ferrous complex* has a quintet ground state. As discussed before, electromer **b** with a doubly filled d_{xz} orbital is predicted at our best theoretical level (R2/B2W) to be the most stable species in the enzyme (QM/MM) while electromer **a** with a doubly filled $d_{x^2-y^2}$ orbital is favored in the gas phase (QM). These two electromers are predicted to have similar isomer shifts, but quite different quadrupole splittings and asymmetry parameters, and it is obvious (Table 10) that only the results for electromer **b** match the experimental Mössbauer data. This confirms that the electromer with a doubly filled d_{xz} orbital is indeed the ground state in the enzyme, consistent with the computed QM/MM energies. The weak temperature dependence of quadrupole splitting observed in the Mössbauer spectrum of

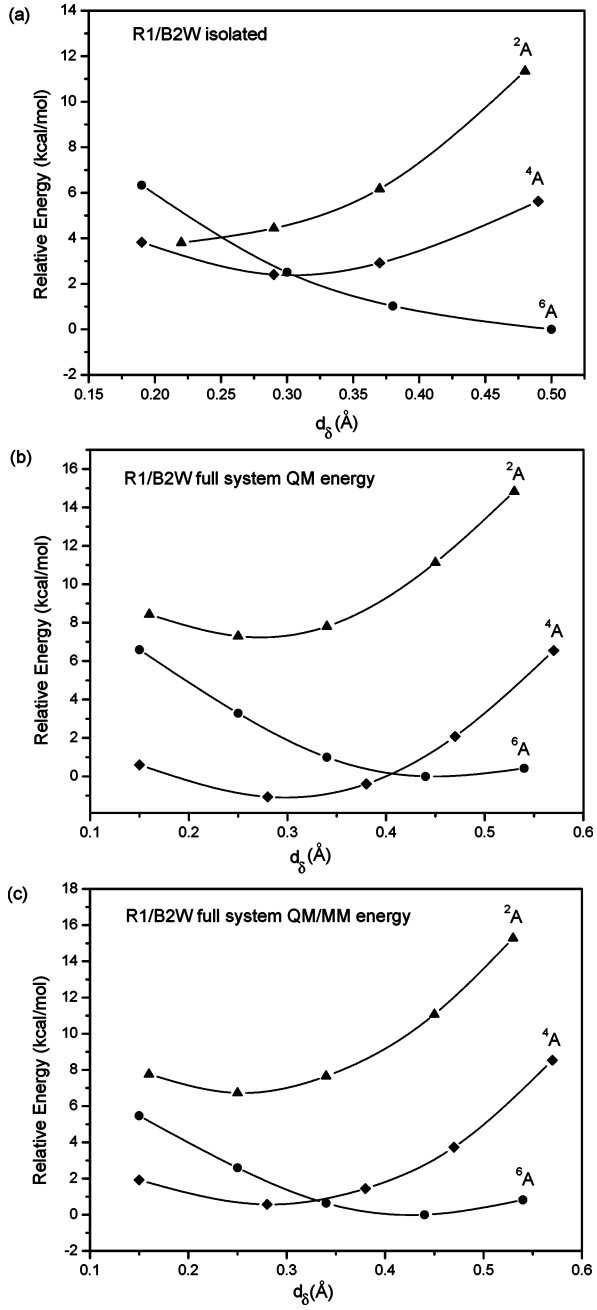

Figure 4. (a) Isolated system QM, (b) full system QM (c), and full system total (QM/MM) energies of sextet (^{6}A), quartet (^{4}A), and doublet (^{2}A) states of ferric pentacoordinated P450$_{cam}$ complex (snapshot 31) as a function of the displacement of the iron atom (d_δ) with respect to the average plane of pyyrole nitrogens computed at the R1/B2W level, using the B3LYP functional (reference energy: the fully optimized sextet state).

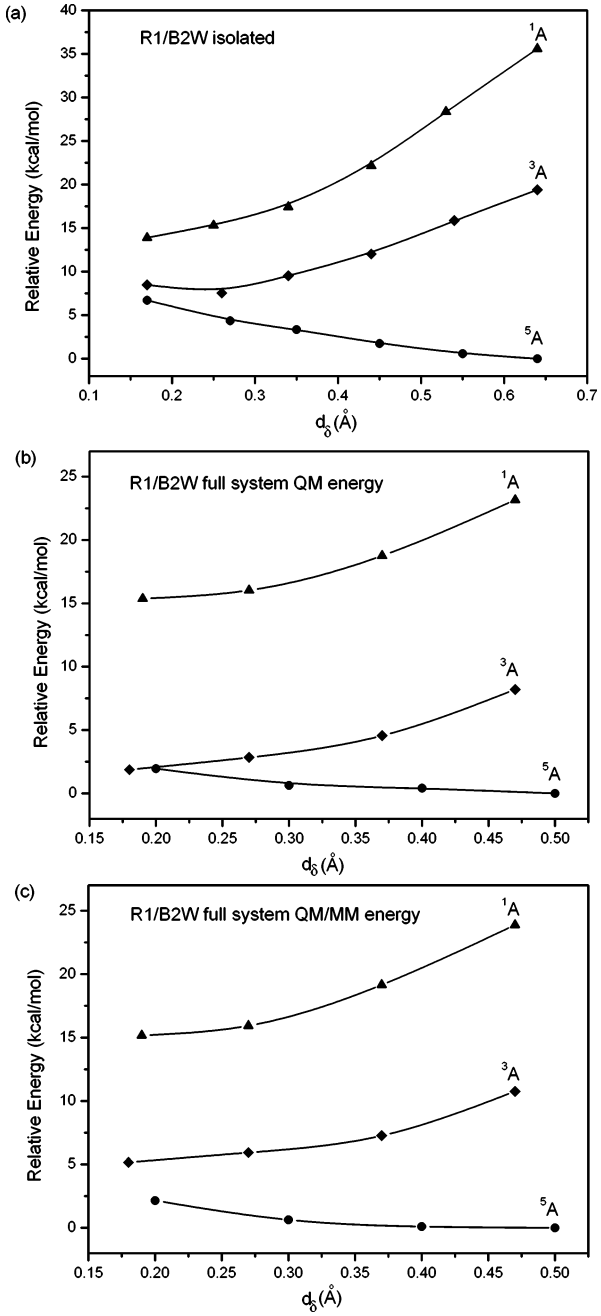

Figure 5. (a) Isolated system QM, (b) full system QM, and (c) full system total (QM/MM) energies of quintet (^{5}A), triplet (^{3}A), and singlet (^{1}A) states of ferrous pentacoordinated P450$_{cam}$ complex (snapshot 31) as a function of the displacement of the iron atom (d_δ) with respect to the average plane of pyyrole nitrogens computed at the R1/B2W level, using the B3LYP functional (reference energy: the fully optimized quintet state).

the *ferrous complex*[7] implies that the quintet ground state does not cross other spin states during the structural fluctuations around equilibrium.

IV. Discussion and Conclusions

The present study shows that relative stabilities of different spin states calculated for heme complexes depend not only on the exact exchange admixture but also on the electron accepting/donating capability of the ligands attached along the axial direction. It has been confirmed that the B3LYP functional is superior to the BLYP and BHLYP functionals for estimating relative stabilities of the title complexes. The dependence of the multiplet splittings on the chosen exchange functional emphasizes the need to calibrate DFT for such applications.

The present B3LYP/MM and gas-phase B3LYP calculations with an all-electron basis set for iron invariably predict the state sequence HS < IS < LS for the pentacoordinated ferric and ferrous complexes. A recent QM/MM (B3LYP/OPLS) study yields a quartet ground state,[17] which is also obtained in the present calculations when using an analogous ECP basis set without polarization functions for iron (LACVP); a larger all-electron basis set for iron is needed in our B3LYP/CHARMM computations to produce a sextet ground state (as observed experimentally). We have found that the amount of stabilization

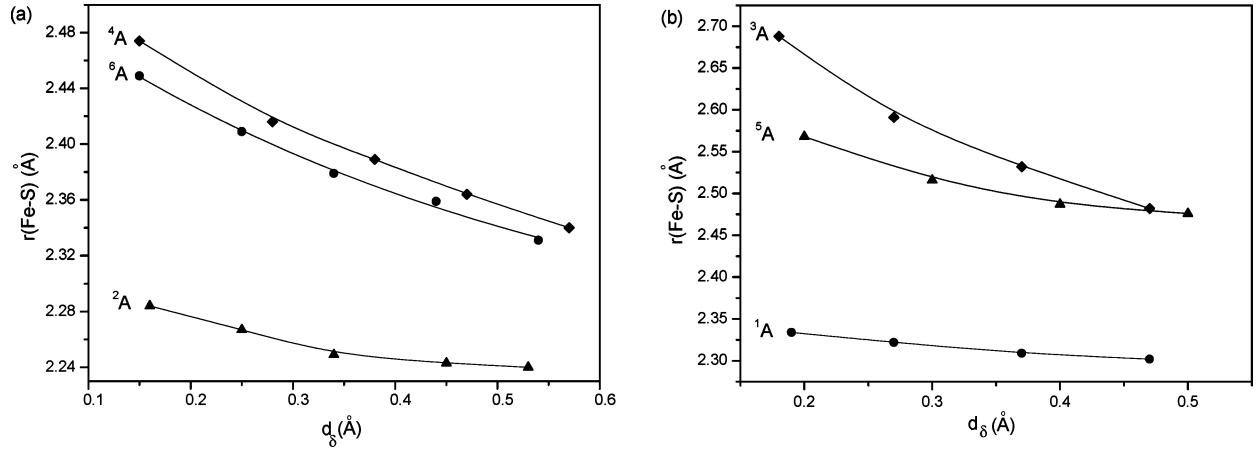

Figure 6. The Fe−S bond length as a function of iron out-of-plane distance computed for the entire (a) ferric and (b) ferrous systems at the R1/B2W level, using the B3LYP functional (snapshot 31).

TABLE 10: Experimental and Computed Mössbauer Isomer Shift δ, Quadrupole Splitting ΔE_Q, and Asymmetry Parameter η of Each Spin State of the Ferric and Ferrous Complexes[a]

complex	state	δ (mm/s)	$\lvert\Delta E_Q\rvert$ (mm/s)	η
ferric	^{6}A(exptl)	0.44	0.79	0.6
	^{6}A	0.42/0.43	0.40/0.24	0.72/0.69
	^{4}A	0.38/0.38	1.74/1.64	0.06/0.14
	^{2}A	0.40/0.39	2.42/2.23	0.64/0.77
ferrous	^{5}A(exptl)	0.82	2.42	0.8
	^{5}A	0.88(0.83)/0.92	4.77(2.83)/4.28	0.08(0.61)/0.07
	^{3}A	0.69/0.66	1.74/1.24	0.53/0.52
	^{1}A	0.65/0.62	1.83/1.91	0.21/0.09

[a] Values refer to the enzyme ($S_{p,p}$)/gas phase ($S_{g,g}$) at the corresponding optimized geometries. The numbers in parentheses belong to the electromer with a doubly filled d_{xz} orbital in the quintet state.

by the protein pocket through the QM contributions follows the order IS > HS > LS (see adiabatic and vertical energies) and correlates with the decrease of the positive spin density on the sulfur atom upon moving from the gas phase to the protein pocket.

Our previous QM/MM calculations on the resting form of P450$_{cam}$ gave a LS (doublet) ground state[20] while our best present QM/MM calculations yield HS ground states for the ferric (sextet) and ferrous (quintet) complexes. The QM/MM calculations thus correctly reproduce the experimentally observed spin state inversion upon substrate binding, indicating that the pentacoordinated complexes become weak-field complexes due to the detachment of axially coordinated water. When an electron is added to the sextet ground state of the ferric complex, it fills the iron $d_{x^2-y^2}$ orbital in the gas phase and the iron d_{xz} orbital in the enzyme. The double occupation of the d_{xz} orbital for the ground-state quintet in the enzyme is indicated by the calculated energetics and confirmed by the comparison of the computed Mössbauer parameters with the experiment.

The experimental reduction potential of the ferric complex (−170 mV) is difficult to reproduce. Estimates based on gas-phase DFT electron affinities are in error by more than 2 V. QM/MM calculations with a protein environment containing charged surface residues (Prot1) yield nonsensical results due to artifacts arising from unphysical long-range electrostatic interactions in the ferrous complex. By contrast, QM/MM computations with a neutral protein environment (Prot2) lead to a differential stabilization of the ferrous complex and thus to a more realistic reduction potential (−0.89 V). The lack of configurational sampling is probably the main cause of the remaining deviation (apart from inherent DFT limitations).

The computed geometry parameters and spin densities for gas-phase models are in agreement with previous gas-phase DFT calculations.[18,19] The most significant geometrical changes upon moving from the gas-phase models to the enzyme occur for the Fe−S bond, which generally becomes somewhat longer, and the iron out-of-plane distance, which is reduced especially for the HS states. The potential energy scans show that the Fe−S bond length decreases with increasing iron out-of plane distance, and the quartet and sextet states can cross in the *ferric complex* through such displacements. The spin states of the *ferrous complex* remain well separated for moderate out-of-plane distortions.

As pointed out before,[17,20,48,49,62,63] the polarizing effect of the enzyme and the presence of H-bond donors in the proximal side stabilize the sulfur p orbitals, and hence the electronic charge on sulfur. As the separation between the sulfur p_z and the iron d_{z^2} orbitals increases in the enzyme, the interaction between these orbitals becomes weaker than in the gas phase. Thus, the Fe(d_{z^2})−S(p_z) σ^* MO (see Scheme 3a) is destabilized less, and its occupation becomes more favored in the enzyme, which leads to the weakening of the Fe−S bond. As a result, the electronic polarization (the QM/MM electrostatic interaction) opposes the stability of the HS states (see the QM contributions to the QM/MM energy in Tables 2 and 4).

In summary, the present QM/MM calculations advance our understanding of how the steric and electrostatic factors in the protein/solvent environment affect the geometrical and electronic structure of the pentacoordinated P450$_{cam}$ complexes. For a given protonation state, different protein/solvent environments taken from two molecular dynamics snapshots give similar relative energies, spin densities, and geometries for each spin state of the ferric and ferrous complexes. Most of these properties are also rather insensitive to the chosen protonation state (Prot1 or Prot2), except for the reduction potential where it is mandatory to use a neutral protein environment with a zero net charge.

Acknowledgment. A.A. thanks Dr. Jan C. Schöneboom, BASF, Ludwigshafen-Germany, for helping in the setup procedure. The authors are grateful to him and to Prof. Sason Shaik for helpful discussions.

Supporting Information Available: Details of the setup procedure, force field parameters, preparatory force field calculations, absolute energies, selected spin densities and structural parameters for the entire system (QM/MM) and for isolated gas-phase structures (QM), and results for larger QM

regions (including camphor and propionate side chains). This material is available free of charge via the Internet at http://pubs.acs.org.

References and Notes

(1) Ortiz de Montellano, P. R., Ed. *Cytochrome P450*: *Structure, Mechanisms, and Biochemistry*, 2nd ed.; Plenum Presss: New York, 1995; Vol. 2.

(2) Mueller, E. J.; Lioda, P. J.; Sligar, S. G. In *Cytochrome P450*: *Structure, Mechanisms, and Biochemistry*, 2nd ed.; Ortiz de Montellano, P. R., Ed.; Plenum Press: New York, 1995; Vol. 2, Chapter 3.

(3) Thomann, H.; Berndardo, M.; Goldfarb, D.; Kroneck, P. M. H.; Ullrich, V. *J. Am. Chem. Soc*. **1995**, *117*, 8243.

(4) Goldfarb, D.; Bernardo, M.; Thomann, H.; Kroneck, P. M. H.; Ullrich, V. *J. Am. Chem. Soc*. **1996**, *118*, 2686.

(5) Tsai, R.; Yu, C. A.; Gunsalus, I. C.; Peisach, J.; Blumberg, W.; Orme-Johnson, W. H.; Beinert, H. *Proc. Natl. Acad. Sci. U.S.A.* **1970**, *66*, 1157.

(6) Sharrock, M.; Debrunner, P. G.; Schulz, C.; Lipscomb, J. D.; Marshall, V.; Gunsalus, I. C. *Biochim. Biophys. Acta* **1976**, *420*, 8.

(7) Debrunner, P. G. In *Iron Porphyrins Part 3*, Physical Bioinorganic Chemistry Series; Lever, A. B. P., Gray, H. B., Eds.; VCH: New York, 1989; Vol. 4, Chapter 2.

(8) Davydov, R.; Makris, T. M.; Kofman, V.; Werst, D. E.; Sligar, S. G.; Hoffman, B. M. *J. Am. Chem. Soc*. **2001**, *123*, 1403.

(9) Sligar, S. G.; Gunsalus, I. C. *Proc. Natl. Acad. Sci. U.S.A.* **1976**, *73*, 1078.

(10) Pochapsky, S. S.; Pochapsky, T. C.; Wei, J. W. *Biochemistry* **2003**, *42*, 5649.

(11) Schlichting, I.; Berendzen, J.; Chu, K.; Stock, A. M.; Maves, S. A.; Benson, D. A.; Sweet, R. M.; Ringe, D.; Petsko, G. A.; Sligar, S. G. *Science* **2000**, *287*, 1615.

(12) Lipscomb, J. D. *Biochemistry* **1980**, *19*, 3590.

(13) de Groot, M. J.; Havenith, R. W. A.; Vinkers, H. M.; Zwaans, R.; Vermeulen, N. P. E.; van Lenthe, J. H. *J. Comput.-Aided Mol. Des.* **1998**, *12*, 183.

(14) Harris, D.; Loew, G. *J. Am. Chem. Soc*. **1993**, *115*, 8775.

(15) Siegbahn, P. E. M.; Blomberg, M. R. A. *Chem. Rev*. **2000**, *100*, 421.

(16) Delaere, D.; Nguyen, M. T. *Chem. Phys. Lett*. **2003**, *376*, 329.

(17) Guallar, V.; Friesner, R. A. *J. Am. Chem. Soc*. **2004**, *126*, 8501.

(18) Ogliaro, F.; de Visser, S. P.; Shaik, S. *J. Inorg. Biochem.* **2002**, *91*, 554.

(19) Rydberg, P.; Sigfridsson, E.; Ryde, U. *J. Biol. Inorg. Chem*. **2004**, *9*, 203.

(20) Schöneboom, J. C.; Thiel, W. *J. Phys. Chem. B* **2004**, *108*, 7468.

(21) Reiher, M.; Salomon, O.; Hess, B. A. *Theor. Chem. Acc*. **2001**, *107*, 48.

(22) Loew, G. H.; Harris, D. L. *Chem. Rev*. **2000**, *100*, 407.

(23) Scherlis, D. A.; Estrin, D. A. *Int. J. Quantum Chem*. **2002**, *87*, 158

(24) Poulos, T. L.; Finzel, B. C.; Howard, A. J. *J. Mol. Biol*. **1987**, *195*, 687.

(25) CHARMM22 force field: MacKerell, A. D., Jr.; Bashford, D.; Bellott, M.; Dunbrack, R. L., Jr.; Evanseck, J. D.; Field, M. J.; Fischer, S.; Gao, J.; Guo, H.; Ha, S.; Joseph-McCarthy, D.; Kuchnir, L.; Kuczera, K.; Lau, F. T. K.; Mattos, C.; Michnick, S.; Ngo, T.; Nguyen, D. T.; Prodhom, B.; Reiher, W. E., III; Roux, B.; Schlenkrich, M.; Smith, J. C.; Stote, R.; Straub, J.; Watanabe, M.; Wiorkiewicz-Kuczera, J.; Yin, D.; Karplus, M. *J. Phys. Chem. B* **1998**, *102*, 3586.

(26) Brooks, B. R.; Burccoleri, R. E.; Olafson, B. D.; States, D. J.; Karplus, M. *J. Comput. Chem*. **1983**, *4*, 187.

(27) Lounnas, V.; Wade, R. C. *Biochemistry* **1997**, *36*, 5402

(28) Becke, A. D. *Phys. Rev. A* **1988**, *38*, 3098.

(29) Becke, A. D. *J. Chem. Phys.* **1993**, *98*, 5648.

(30) Becke, A. D. *J. Chem. Phys.* **1993**, *98*, 1372.

(31) Lee, C.; Yang, W.; Parr, R. G. *Phys. Rev. B* **1988**, *37*, 785.

(32) Antes, I.; Thiel, W. *Hybrid Quantum Mechanical and Molecular Mechanical Methods*; Gao, J., Ed.; ACS Symp. Ser. 712; American Chemical Society: Washington, DC, 1998; pp 50−65.

(33) Hay, J. P.; Wadt, W. R. *J. Chem. Phys*. **1985**, *82*, 299.

(34) (a) Wachters, A. J. H. *J. Chem. Phys.* **1970**, *52*, 1033. (b) Hay, P. J. *J. Chem. Phys.* **1977**, *66*, 4377. (c) Bauschlicher, C. W., Jr.; Langhoff, S. R.; Barnes, L. A. *J. Chem. Phys.* **1989**, *91*, 2399.

(35) (a) Ditchfield, R.; Hehre, W. J.; Pople, J. A. *J. Chem. Phys*. **1971**, *54*, 724. (b) Hehre, W. J.; Ditchfield, R.; Pople, J. A. *J. Chem. Phys*. **1972**, *56*, 2257. (c) Hariharan, P. C.; Pople, J. A. *Theor. Chim. Acta* **1973**, *28*, 213. (d) Clark, T.; Chandrasekhar, J.; Spitznagel, G. W.; Schleyer, P. v. R. *J. Comput. Chem*. **1983**, *4*, 294.

(36) (a) Schäfer, A.; Horn, H.; Ahlrichs, R. *J. Chem. Phys.* **1992**, *97*, 2571. (b) Schäfer, A.; Huber, C.; Ahlrichs, R. *J. Chem. Phys*. **1994**, *100*, 5829.

(37) Bakowies, D.; Thiel, W. *J. Phys. Chem*. **1996**, *100*, 10580.

(38) de Vries, A. H.; Sherwood, P.; Collins, S. J.; Rigby, A. M.; Rigutto, M.; Kramer, G. J. *J. Phys. Chem. B* **1999**, *103*, 6133.

(39) Sherwood, P.; de Vries, A. H.; Guest, M. F.; Schreckenbach, G.; Catlow, C. R. A.; French, S. A.; Sokol, A. A.; Bromley, S. T.; Thiel, W.; Turner, A. J.; Billeter, S.; Terstegen, F.; Thiel, S.; Kendrick, J.; Rogers, S. C.; Casci, J.; Watson, M.; King, F.; Karlsen, E.; Sjovoll, M.; Fahmi, A.; Schäfer, A.; Lennartz, C. *J. Mol. Struct.* (*THEOCHEM*) **2003**, *632*, 1.

(40) ChemShell is a modular QM/MM program developed in the European QUASI project under the coordination of P. Sherwood. See: http://www.cse.clrc.ac.uk/qcg/chemshell.

(41) (a) Ahlrichs, R.; Bär, M.; Häser, M.; Horn, H.; Kölmel, C. *Chem. Phys. Lett.* **1989**, *162*, 165. (b) Ahlrichs, R.; Bär, M.; Baron, H.-P.; Bauernschmitt, R.; Böcker, S.; Ehrig, M.; Eichkorn, K.; Elliot, S.; Furche, F.; Häser, M.; Horn, H.; Hättig, C.; Huber, C.; Huniar, U.; Kattanneck, M.; Köhn, A.; Kölmel, C.; Kollwitz, M.; May, K.; Ochsenfeld, C.; Öhm, H.; Schäfer, A.; Schneider, U.; Treutler, O.; v. Arnim, M.; Weigend, F.; Weis, P.; Weiss, H. TURBOMOLE 5.5, University of Karlsruhe, 2002.

(42) Smith, W.; Forester, T. *J. Mol. Graph.* **1996**, *14*, 136.

(43) Billeter, S. R.; Turner, A. J.; Thiel, W. *Phys. Chem. Chem. Phys*. **2000**, *2*, 2177.

(44) Neese, F. ORCA-an ab initio, DFT and semiempirical electronic structure package, Version 2.2, Revision 14; Max-Planck-Institut für Strahlenchemie: Mülheim an der Ruhr, Germany, 2002.

(45) Neese, F. *J. Chem. Phys.* **2003**, *118*, 3939.

(46) Neese, F. *Curr. Opin. Chem. Biol*. **2003**, *7*, 125.

(47) Neese, F. *Inorg. Chim. Acta* **2002**, *337*, 181.

(48) Schöneboom, J. C.; Lin, H.; Reuter, N.; Thiel, W.; Cohen, S.; Ogliaro, F.; Shaik, S. *J. Am. Chem. Soc*. **2002**, *124*, 8142.

(49) Green, M. T. *J. Am. Chem. Soc*. **1998**, *120*, 10772.

(50) Rovira, C.; Kunc, K.; Hutter, J.; Ballone, P.; Parrinello, M. *J. Phys. Chem. A* **1997**, *101*, 8914.

(51) Obara, C.; Kashiwagi, H. *J. Chem. Phys*. **1982**, *77*, 3155.

(52) Salomon, O.; Reiher, M.; Hess B. A. *J. Chem. Phys.* **2002**, *117*, 4729.

(53) Time-dependent DFT calculations with the B3LYP functional using the ESCF module of TURBOMOLE (Bauernschmitt, R.; Ahlrichs, R. *Chem. Phys. Lett.* **1996**, *256*, 454) for the open-shell systems yielded only positive excitation energies, confirming that the electronic configurations obtained are the ground states. The expectation values of S^2 computed for the doublet state with B1L and B2L basis sets were typically 0.8−1.0 (ideally 0.75), indicating only minor spin contamination, while the doublet state was calculated to be pure with B2W basis. The doublet state energies were not corrected by any of the available spin projection schemes. All the HS and IS species were found to be pure spin states.

(54) Reiss, H.; Heller, A. *J. Phys. Chem*. **1985**, *89*, 4207.

(55) Crystal, J.; Friesner, R. A. *J. Phys. Chem. A* **2000**, *104*, 2362.

(56) Curtiss, L. A.; Redferm, P. C.; Raghavachari, K.; Pople, J. A. *J. Chem. Phys.* **1998**, *109*, 42.

(57) Gill, P. M. W.; Johnson, B. G.; Pople, J. A. *J. Chem. Phys. Lett.* **1992**, *197*, 499.

(58) Olsson, M. H.; Hong, G.; Warshel, A. *J. Am. Chem. Soc*. **2003**, *125*, 5025.

(59) Li, G.; Zhang, X.; Cui, Q. *J. Phys. Chem. B* **2003**, *107*, 8643.

(60) Amara, P.; Field, M. J. *Theor. Chem. Acc.* **2003**, *109*, 43.

(61) Champion, P. M.; Lipscomb, J. D.; Münck, E.; Debrunner, P. G.; Gunsalus, I. C. *Biochemistry* **1975**, *14*, 4151.

(62) Sigman, J. A.; Pond, A. E.; Dawson, J. H.; Lu, Y. *Biochemistry* **1999**, *38*, 11122.

(63) (a) Ogliaro, F.; Cohen, S.; de Visser, S.; Shaik, S. *J. Am. Chem. Soc*. **2000**, *122*, 12892. (b) Ogliaro, F.; Cohen, S.; Filatov, M.; Harris, N.; Shaik, S. *Angew. Chem., Int. Ed.* **2000**, *39*, 3851. (c) Ogliaro, F.; Harris, N.; Cohen, S.; Filatov, M.; de Visser, S.; Shaik, S. *J. Am. Chem. Soc*. **2000**, *122*, 8977. (d) Ogliaro, F.; de Visser, S.; Shaik, S. *J. Inorg. Biochem.* **2003**, *91*, 554.